Some of the numerical methods discussed in this volume have not yet seen their full development. The thrust of future research will be to use seismological measurements to infer the physical properties of more realistic and refined three-dimensional Earth models. Lateral variation in upper mantle structure, oceanic–continental boundaries, plate boundaries, and mountain roots will be studied quantitatively for the first time using surface-wave dispersion. The effect of soils and local geological structure on strong earthquake shaking will be predicted by numerical methods.

# Finite Difference Methods for Seismic Wave Propagation in Heterogeneous Materials

DAVID M. BOORE

NATIONAL CENTER FOR EARTHQUAKE RESEARCH
U.S. GEOLOGICAL SURVEY
MENLO PARK, CALIFORNIA



## I. Introduction

AS MOST OF THE chapters in this book indicate, seismologists usually model the velocity and density structure of the earth with heterogeneity in the vertical direction only. Mathematical solutions for wave propagation in such models are relatively straightforward. There are a number of important problems in seismology, however, for which lateral changes in material properties are significant. Because the geometry in these cases cannot be represented as normal surfaces in a system of separable coordinates the solution of the direct problem is not simple, and some type of perturbation or numerical solution is necessary.

A number of different numerical schemes of varying complexity have been used to solve elastic wave propagation problems. In a continuing series of papers Alterman and her co-workers have used a simple finite difference method to solve the vector elastic equations of motion when subject to some specific initial and boundary conditions (Alterman and Karal, 1968; Alterman and Aboudi, 1969; Alterman *et al.*, 1972; see chapter by Alterman and Loewenthal in Volume 12 for a more complete list of Alterman's papers). This method was also used by Bertholf (1967) to solve for the transient displacements in an elastic finite cylindrical bar subjected to applied stresses at one end. Plamondon (1966) used a different, more complex method to compute the motion due to a spherical source beneath the earth's surface. Even more involved methods, which are capable of following the motion through regions of plastic, shock, or brittle behavior, have been devised by Maenchen and Sack (1963) and Petschek and Hansen (1968), among others. Another computational scheme which has been very successful in studying eigenvibration problems and is currently attracting much attention in seismology is the finite element method (see chapter by Lysmer and Drake, this volume).

Two other recently developed methods (not discussed in this volume) for wave propagation in laterally heterogeneous media are the wave scattering method of Aki and Larner (1970; Larner, 1970) and the perturbation method of Claerbout (1970a, b, 1971), Claerbout and Johnson (1972), and Landers (1971). These methods, potentially very valuable, have received little attention up to this time.

The usefulness of any of the above schemes depends greatly on the problem being solved; one must choose that method which gives reasonable answers with the least amount of storage space and computer time. The straightforward finite difference method discussed in this chapter is a practical way of solving a number of pertinent seismological problems. The essence of this technique is to replace the differential equations and boundary conditions by simple finite difference approximations in such a way that an explicit, recursive set of equations is formed. This results in a time-marching procedure which can be used to solve for the displacements at each grid point as a function of time given the motion at the first two time steps.

There are many advantages to the finite difference method discussed in this article. Some of these are that it is very easy to program, many different problems can be solved with only minor alterations of the program, and the preparation of input data for a particular problem is not tedious. Furthermore, as opposed to steady-state solutions, the use of transient signals gives information at many frequencies from one computer run. The transient signal, in combination with the explicit set of equations, also makes the treatment of artificial boundaries (required by computer storage space limitations) more natural and less worrisome than in most other numerical schemes. Another convenient feature is that displacements as a function of time at a given site or pictures of the total wave field at a given time can be obtained with equal ease.



The finite difference method will probably find its greatest use in solving problems not possessing analytical solutions, but it can also compete with the analytical solutions, especially when such solutions require the evaluation of complicated series expansions (Alterman and Karal, 1968). The ease with which it can be programmed makes the finite difference method an excellent pedagogical tool in illustrating concepts of wave propagation in a dynamic, controllable manner. It is particularly useful for this if propagation is restricted to one dimension only, for then the computations are very rapid.

The technique is limited, for practical reasons, to certain classes of problems. It is difficult to enumerate these here, but in a general way we can say that it is most useful in the near field region of sources, where the sources can be either real or, as in this chapter, effective sources introduced by complexities along the travel path. Thus, for example, it would be impractical to use the finite difference method to evaluate the surface displacements of a short period body wave incident upon an irregular crust–mantle interface. On the other hand, it is ideal for the solution of a layered model in which the layer thicknesses are on the order of the seismic wavelengths.

Finite difference methods for problems involving partial differential equations have been developed and used for years in such disciplines as meteorology and civil and mechanical engineering. To be useful in seismological problems, however, wave propagation in models having material property variations in at least two spatial dimensions must be treated. This requires large amounts of computer space and rapid calculations, and it was only several years ago that machines capable of handling such problems were commonly available (one of the first papers dealing with numerical wave propagation to appear in the seismological literature was by Cherry and Hurdlow in 1966). Although there is no lack of possible methods based on finite differences, relatively few have actually been tested and applied to nontrivial seismological problems. It is the goal of this chapter to present in detail the methods used and experience gained by the author in making several of these applications, with the hope that it will stimulate others to explore further the uses of the method. Several improvements included here have not been discussed by the author in previous publications. Theoretical aspects of finite difference solutions to partial differential equations have been avoided. For these, reference should be made to one of the textbooks on the subject (e.g., Richtmeyer and Morton, 1967).

## II. Method

### A. Assumptions

The basic problem concerns transient wave propagation in a semi-infinite half-space bounded by a stress free surface. The free surface need not be planar nor must the material making up the half-space be homogeneous. The material through which the waves propagate is assumed to be isotropic and linearly elastic (the treatment of viscoelastic material is discussed briefly in Section III,A). Because of storage space and computation time limitations we assume that all variations in material properties, boundaries, and wavefields take place in only two spatial directions ($x$, $z$).

With these assumptions the general elastic motion can be uncoupled into two types: horizontal shear motion (SH), characterized by displacements $v$ in the $y$ direction only, and coupled compressional and shear motion involving the $x$, $z$ components of displacements $u$, $w$. Although many of the methods discussed below can be applied to the complete vector equation, this chapter will be concerned exclusively with SH motion. One of the primary reasons for this is that less storage space and computer time are required than in the corresponding vector elastic case, and thus more realistic heterogeneities can be modeled within the space–time limits available. Furthermore, the seismic radiation from earthquakes usually contains a significant amount of SH motion and it is SH motion that is of greatest interest in engineering seismology.

### B. Derivative Approximations

#### 1. *Standard Formulas*

The basis of the finite difference technique is the replacement of differential operators by difference approximations. These approximations can be found in a number of ways; here we only intend to introduce notation and present some formulas. Further details may be found in textbooks such as Smith (1965) and Mitchell (1969).

The continuous $x, z, t$ space is divided into rectangular blocks. The displacement field is then specified by values at the discrete set of nodepoints represented by the corner intersections of the blocks. For constant $x$, $z$, and $t$ spacing $\Delta x$, $\Delta z$, and $\Delta t$, any node is uniquely determined with reference to an arbitrary coordinate origin by the indices $m$, $n$, $p$. Thus $v^p_{m,n} = v(m\,\Delta x, n\,\Delta z, p\,\Delta t)$, where subscripts refer to spatial location and superscripts to time. The absence of an index implies that the variable represented by that index can take continuous values, as in $v_{m,n} = v(m\,\Delta x, n\,\Delta z, t)$. When interface



conditions are discussed at a boundary between two media, the subscripts 1 and 2 will sometimes be used to denote the respective media. No confusion should exist with the more usual subscripts representing spatial location. As a final piece of nomenclature, in future discussions the term "computational star" will be used; this refers to the spatial pattern of gridpoints used in the difference approximation of a differential operator.

With the above notation, standard centered approximations for first and second derivatives are

$$(\partial v/\partial x)_m \simeq (v_{m+1/2} - v_{m-1/2})/\Delta x, \tag{1}$$

$$(\partial^2 v/\partial x^2)_m \simeq (v_{m+1} - 2v_m + v_{m-1})/(\Delta x)^2. \tag{2}$$

Another centered approximation to the first derivative is

$$(\partial v/\partial x)_m \simeq (v_{m+1} - v_{m-1})/2\Delta x. \tag{3}$$

We will also use single-sided approximations, such as

$$(\partial v/\partial x)_m \simeq (v_{m+1} - v_m)/\Delta x, \tag{4}$$

to the first derivative. These are of a lower order of accuracy than the centered approximations in Eqs. (1) and (3).

All of the above formulas apply, with obvious changes, to derivatives with respect to $z$ and $t$. Formulas for nonconstant $\Delta x$, $\Delta z$, and $\Delta t$ can also be found easily (e.g., Boore, 1970b; Rowe, 1955). For example, the formula for the second $x$-derivative is

$$\left(\frac{\partial^2 v}{\partial x^2}\right)_m \simeq 2\left[\frac{v_{m+1}}{h_2(h_1+h_2)} - \frac{v_m}{h_1 h_2} + \frac{v_{m-1}}{h_1(h_1+h_2)}\right], \tag{5}$$

where $h_1$, $h_2$ are the spacings between nodes $m-1$, $m$ and $m$, $m+1$.

#### 2. *Attempted Use of Splines*

For the wave equation in a homogeneous material we seek an approximation to the Laplacian operator acting on the displacement field at a given time. This is obtained by using Eq. (2) and a corresponding expression for the second $z$-derivative. Since one way of obtaining Eq. (2) is to differentiate an interpolating quadratic polynomial fit to the three points $m-1$, $m$, $m+1$, one might wonder if a better interpolating polynomial could be found which would give similar accuracy but with larger grid spacings. In this way a given

spatial area could be represented by a smaller number of grid points and thus the computation time, which is proportional to the number of grid points, would be reduced. As an exploratory attempt, bicubic spline functions (Bhattacharyya, 1969) were fit to sets of points obtained by digitizing three cycles of a sine wave at different rates. Derivatives of the resulting spline function, evaluated at the node points, and difference approximations using Eq. (3) and Eq. (2) on the tabulated set of points from which the spline was generated, were then compared with the exact values. Figure 1 shows a measure of the mean percentage error, averaged over the second cycle (in order to avoid end condition effects) of the sine wave, as a function of digitized

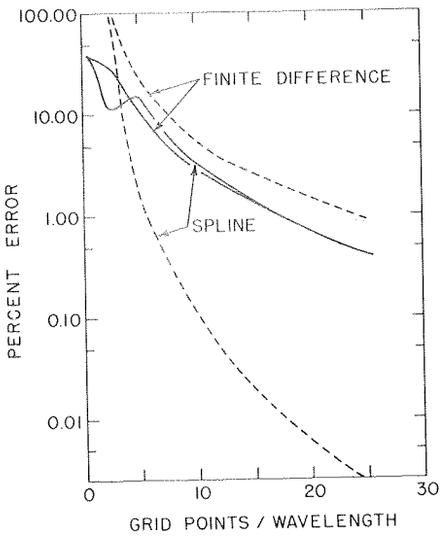


FIG. 1. The mean error, as a function of sampling rate, from spline and finite difference approximations to the first (---) and second (—) derivatives of a sine function.

points per wavelength. The spline gives a better approximation to the first derivative, but surprisingly, both the spline and finite difference approximation of the second derivative are nearly equivalent. Thus no obvious advantage would seem to accrue from splines as used here, especially considering that a matrix inversion (albeit a rapid one) is needed to generate the spline function. Splines, however, are finding utility in other areas of seismology, such as in the smoothing of travel time tables (Curtis and Shimshoni, 1970), calculation of divergence factors (Shimshoni and Ben-Menahem, 1970),



calculation of ray theory amplitudes (Moler and Solomon, 1970), and location of small earthquakes (Wesson, 1971). The negative result obtained here does not imply that splines are not useful in other ways in the numerical solution of differential equations; books such as Schoenberg (1969) contain references to such techniques.

Disregarding splines, Fig. 1 shows the effect of grid spacing on the accuracy of the finite difference approximations (2) and (3). For example, at least 7 points are required per wavelength in order to obtain an accuracy of 95% in the second derivative. More discussion about the wavelength–gridspacing relationship will be found in Section II,E,1.

## C. Equations of Motion

The basic equation for the displacement $v$ in an inhomogeneous medium is

$$\rho \frac{\partial^2 v}{\partial t^2} = \frac{\partial}{\partial x}\left(\mu \frac{\partial v}{\partial x}\right) + \frac{\partial}{\partial z}\left(\mu \frac{\partial v}{\partial z}\right), \tag{6}$$

where $\mu(x, z)$ is the rigidity of the material and $\rho(x, z)$ is the density. Body forces ($f$) have been neglected; if present, an additional term $\rho f$ would be added to the right-hand side. Since wave propagation through homogeneous material joined along discrete interfaces is of most interest, a discussion of the general heterogeneous equation of motion will be deferred until the next section (which deals with boundary conditions). In a homogeneous material Eq. (6) becomes

$$\rho\, \partial^2 v/\partial t^2 = \mu \nabla^2 v. \tag{7}$$

where $\nabla^2$ is the Laplacian operator. Replacing the derivatives by the difference approximation in Eq. (2), and gathering all the terms at time levels $p, p-1$ on the right-hand side, gives, as an approximation to Eq. (7),

$$v_{m,n}^{p+1} = 2v_{m,n}^{p} - v_{m,n}^{p-1} + \beta^2 \Delta t^2 \times \left[\frac{v_{m+1,n}^{p} - 2v_{m,n}^{p} + v_{m-1,n}^{p}}{(\Delta x)^2} + \frac{v_{m,n+1}^{p} - 2v_{m,n}^{p} + v_{m,n-1}^{p}}{(\Delta z)^2}\right], \tag{8}$$

where $\beta = (\mu/\rho)^{1/2}$ is the shear wave velocity. This is the basic equation used in the computations. It is explicit in the displacement at the new time level $p+1$, and it is recursive; given initial displacements at two consecutive time points it is a simple matter to compute displacements at any other time by a forward time-marching process.

In common with most explicit finite difference approximations to partial differential equations, a condition relating the time and space grid intervals must be satisfied if the solution to the difference equations is to be stable. For the wave equation, this condition in practice is not excessively restrictive. This is in contrast to the heat flow equation, where the stability condition is so restrictive that implicit, unconditionally stable methods such as the alternating direction implicit scheme (Mitchell, 1969) must be used.

Various implicit methods, based on splitting the two-dimensional problem into several problems implicit in one direction only, do exist for the wave equation; Mitchell (1969) gives a thorough discussion of these schemes. Some are unconditionally stable and others, although requiring stability relations, are highly accurate. These schemes are all implicit and require a number of tridiagonal matrix inversions, for which there are very rapid algorithms, to progress from one time step to the next. Although more complicated than the explicit scheme given in Eq. (8), these methods may be useful in certain classes of problems. Because these schemes are in large part untested, however, there is a need for experimentation to determine their usefulness and limitations.

## D. Boundary Conditions

### 1. *Physical Boundaries*

Although Eq. (6) in combination with initial conditions completely defines the problem, a special case arises where a discrete change in rigidity occurs across some surface in the body. Then Eq. (6) implies both

$$(\mu\, \partial v/\partial n)_+ = (\mu\, \partial v/\partial n)_-, \tag{9}$$

where $\partial/\partial n$ is a derivative normal to the interface, and $v_+ = v_-$. These conditions can also be expressed as the continuity of normal stress and displacement across the interface.

The explicit boundary condition at the stress free surface is

$$(\partial v/\partial n)_{\text{surf.}} = 0. \tag{10}$$

We can get this from Eq. (9) by assuming $(\mu)_- = 0$.

Most published applications of the finite difference method to elastic wave propagation involve plane, rather than curved, interfaces. For these, a number of methods which involve explicit approximation to the interface boundary condition (9) can be devised (Alterman and Karal, 1968; Bertholf, 1967; Boore, 1970a; Chiu, 1965). These approximations, however, are difficult to generalize to curved interfaces, and for this reason a relatively crude but adequate method was derived by the author. For want of a better name, this was called the explicit continuous stress method. Recently, several methods based on the heterogeneous wave equation have been investigated, and these appear to be superior in every respect to the explicit continuous stress method. Both of these approaches to curved boundaries are discussed below. Since these methods also work for plane interfaces (which are just a particular form of a curved boundary), the more specialized plane interface methods mentioned above will not be discussed.



a. *Heterogeneous Media Approach.* The interface condition (9) can be derived by considering the behavior of the equation describing the motion of a heterogeneous material, Eq. (6), as the distance over which the rigidity change occurs decreases to zero. This suggests that a natural way of treating the interface is to write approximations to Eq. (6) at the grid points near the interface. Two approximations are given below, and both reduce to Eq. (8) when the medium has uniform properties.

We are concerned only with the approximation of the right-hand side of Eq. (6); the time derivative can be replaced by the standard centered difference approximation. If the first derivative operator (1) is applied consecutively, the $x$-derivative is given by

$$\frac{\partial}{\partial x}\left(\mu \frac{\partial v}{\partial x}\right) \simeq \frac{\mu_{m+1/2}\, v_{m+1} - (\mu_{m+1/2} + \mu_{m-1/2}) v_m + \mu_{m-1/2}\, v_{m-1}}{(\Delta x)^2}. \tag{11}$$

The approximation of the $z$-derivative is similar. Since we have detailed knowledge of the rigidity for any point in space, evaluating it midway between grid points, as implied by $\mu_{m+1/2}$ and $\mu_{m-1/2}$, is not a problem.

Another approach which depends more on the detailed variation of $\mu(x, z)$ is due to Tikhonov and Samarskii (Mitchell, 1969, p. 23). To start, a variable $w$, defined by

$$w = -\mu(\partial v/\partial x), \tag{12}$$

is introduced. The equation above is rewritten

$$w/\mu = -\partial v/\partial x \tag{13}$$

and integrated over the interval $[(m-1)\,\Delta x, m\,\Delta x]$. Replacing $w$ by a constant "mean-value" $w_{m-1/2}$ gives

$$w_{m-1/2} \int_{x_{m-1}}^{x_m} \frac{dx}{\mu(x, z)} = -(v_m - v_{m-1}), \tag{14}$$

and similarly for $w_{m+1/2}$. These equations can be solved for $w_{m-1/2}$ and $w_{m+1/2}$. Since

$$\frac{\partial}{\partial x}\left(\mu \frac{\partial v}{\partial x}\right)_m = -\left(\frac{\partial w}{\partial x}\right)_m \simeq \frac{w_{m-1/2} - w_{m+1/2}}{\Delta x} \tag{15}$$

we have finally

$$\frac{\partial}{\partial x}\left(\mu \frac{\partial v}{\partial x}\right)_m \simeq \frac{(A_m v_{m-1} - (A_m + A_{m+1})v_m + A_{m+1}v_{m+1}}{(\Delta x)^2}, \tag{16}$$

where

$$A_l = \Delta x \left[\int_{x_{l-1}}^{x_l} \frac{dx}{\mu}\right]^{-1}. \tag{17}$$

Similar formulas hold for the $z$-dependence. In effect, the heterogenous methods given by Eq. (11) and Eq. (16) determine equivalent values of rigidity at the node points in the computational stars; derivatives of the rigidity are never taken explicitly. For a given computational star it is natural to define, as shown in the inset in Fig. 2, the equivalent rigidities as $\mu_N, \mu_S, \mu_E, \mu_W$).

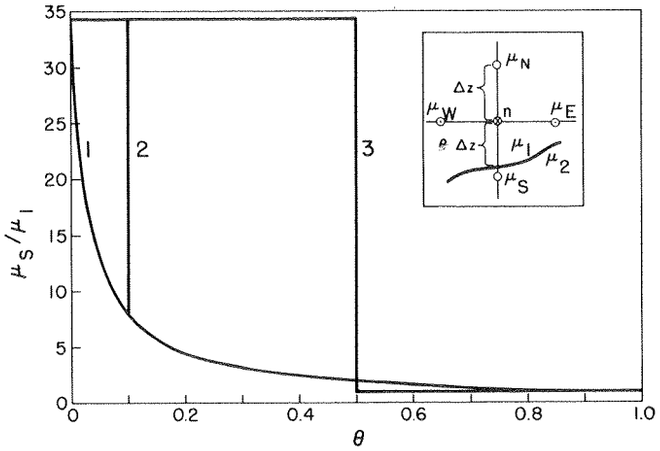


FIG. 2. The equivalent rigidity at the "southern" point of the computational star placed at $n$ (see inset). In this example the curve intersects only the southern leg of the computational star. Curve 1 is for Eq. (18) and curve 3 is for Eq. (11). Curve 2 is a modification of curve 1.



The formulas (11) and (16) hold for any arbitrary rigidity dependence. When the rigidity has a step change in value, as when two homogeneous materials are joined together, the integration in Eq. (17) can be performed explicitly. Then, referring to the gridpoint–interface relation shown in the inset to Fig. 2, we have

$$A_{n+1} = \mu_S = \frac{1}{(\theta/\mu_1) + (1-\theta)/\mu_2}, \tag{18}$$

where $\theta\,\Delta z$ is the distance from the center point to the interface. Also note that for the specific grid–interface relation shown $A_n = \mu_N = \mu_1$ and $\mu_E = \mu_W = \mu_1$. The equivalent rigidity $\mu_S$, as given by (18) and as implied in Eq. (11) (curves 1 and 3, respectively), is graphed as a function of $\theta$ in Fig. 2 for values of $\mu_1$ and $\mu_2$ used in the second example in Section IV,B,1. Curve 2 in the figure is the result of assigning $\theta = 0$ whenever $\theta$ is less than 0.1. The difference between the curves 1 and 2 and curve 3 is considerable, but seems to have little effect on the results.

A special interpretation must be given Eq. (17) when the path of integration coincides with a boundary separating media of different rigidities. One possibility is to assume a wavy interface that is alternately above and below consecutive gridpoints; then letting $\theta = 0.5$ in Eq. (18) would be appropriate. Another possibility is to assume $\mu = (\mu_1 + \mu_2)/2$ along the path of integration. For several reasons the latter choice seems to be proper: it gives better answers when applied to Love wave propagation on a flat layer, and gives an equation which is identical to those derived from two different approximations of the explicit interface condition.

As noted before, the free surface boundary condition is a special case of the interface condition; thus, the interface conditions along a free surface of varying shape can be treated using the heterogeneous media approach if we consider the air above the surface to be a uniform material of zero rigidity.

b. *Explicit Continuous Stress Method.* This method is best explained with reference to Fig. 3. For certain grid points, such as A or A′, the Laplacian cannot be approximated by a regular star wholly contained within one medium. The Laplacian at these interface points can be written, using Eq. (5), in terms of an irregular star with short legs. This star will involve displacements at actual grid points and at "curve points" defined by interface–grid line intersections. In Fig. 3, point D is one of the two curve points required for the irregular star placed at A. Assuming that displacements are known at all grid points and curve points at times $p, p-1$, the difference equation can be used to generate new displacements at time $p+1$ for all

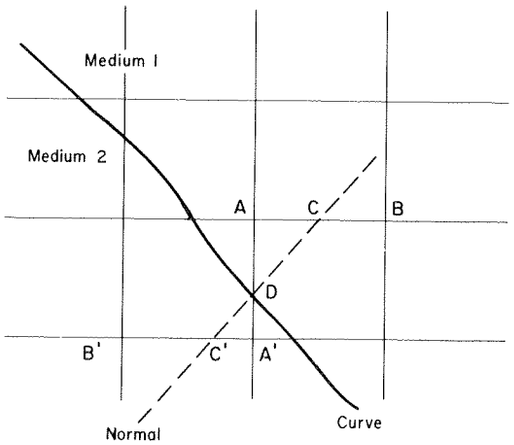


FIG. 3. A portion of the spatial grid near a curved boundary. The labeled points are referred to in Section II,D,1,b (from Boore, 1970b).

but the curve points. The new curve point values are given by approximating the explicit interface condition (9) in the following manner:

(1) A normal to the curve is constructed at D.

(2) The displacements at the normal–grid line intersection C is determined by linear interpolation between grid points A and B (and similarly for C′).

(3) An approximation to the interface equation, given by

$$\mu_1 \frac{v_D^{p+1} - v_C^{p+1}}{DC} = \mu_2 \frac{v_{C'}^{p+1} - v_D^{p+1}}{DC'}, \tag{19}$$

where DC, DC′ are the lengths along the normal from C, C′ to D, is used to obtain the new curve point displacement $v_D^{p+1}$. The curve point values are not required to satisfy explicitly the wave equation, but are given as weighted averages of nearby points which do; thus, in a uniform material the equation used at the curve point will not reduce to the usual equation of motion.

As discussed in Section II,F,2, a local instability usually is produced by the short legs in the irregular computational star near the interface. This instability is sometimes, but not always, a problem, and two devices are used to make it less so. The first is to deform the curve so that it passes through any grid point which is less than a specified distance from the curve; the grid point is then treated as a curve point, and an approximation to the Laplacian is not used. This eliminates very short legs. The second procedure is simply to decrease the time spacing so that it more closely approximates the time step required by the local stability condition. This, of course, can



be very costly, and is a major reason that the heterogeneous approaches discussed above are more desirable. The heterogeneous approaches are also superior because they are more general and are easier to program.

### 2. *Artificial Boundaries*

Because of the limitations of finite computer storage, it is obvious that wave propagation in a medium unbounded in any direction cannot be modeled. Artificial boundaries must be introduced. This places some definite constraints on the length of time for which the computed solution can be considered free of contamination. Since the manner in which the artificial boundaries are treated is dependent on the problem, a general treatment of these boundaries cannot be given; instead, a specific example will be discussed to illustrate some of the possibilities.

The example is that of SH body waves vertically incident from below on a crust or surficial layer with a localized, irregular but symmetric interface (Fig. 4). The vertical and bottom boundaries shown in the figure are all

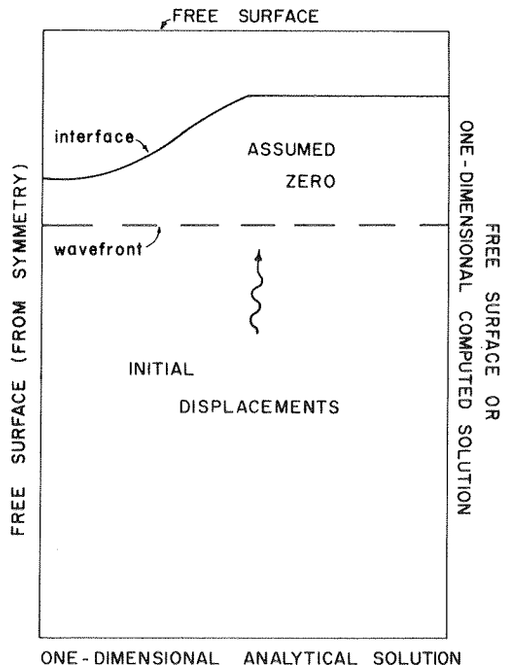


FIG. 4. SH body waves incident on a symmetric basin. Shown are the conditions used at the artificial boundaries and the location of the initial displacement. Adapted from Boore *et al.* (1971).

artificial, in the sense used above. The symmetric structure and vertical incidence enables us to solve for the motion in just half the region, as shown, with the condition $\partial v/\partial x = 0$ at the left boundary (plane of symmetry), thus treating it as a free surface. The displacements along the right boundary can be given in several ways. If, as at the bottom of Fig. 5, the irregularity in the structure is assumed to be periodic, then the right boundary also can be treated as a free surface. Another approach is to give the right-hand boundary displacements as a function of time by the numerical solution to an auxiliary one-dimensional problem of SH waves vertically incident on a flat layer of appropriate thickness. This is an attempt to approximate wave propagation in the real, nonperiodic model. The numerical rather than the analytical solution is used because of the time–space limitations required by the Fourier synthesis in the analytical solution. The displacements along the bottom are given by the analytical solution to the one-dimensional problem. This solution, which requires one Fourier synthesis at the beginning of the program, is used both for the regular and auxiliary problems.

The methods above for the artificial boundaries are only approximate (except for the left-hand symmetry condition). The differences between the computed solution and the actual solution that would exist in the absence of the boundaries act as secondary sources and produce spurious reflections which contaminate the solutions at the surface. The secondary sources are

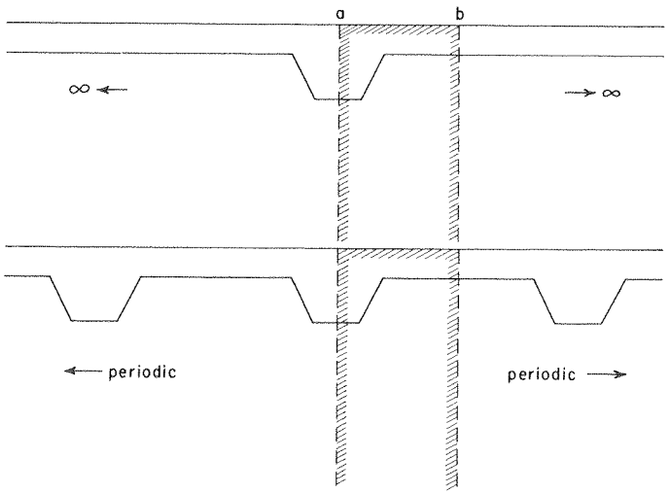


FIG. 5. Models implied by artificial boundary conditions if (*lower*) the free surface condition is used at b, and (*upper*) if the solutions to the auxiliary problem are used at b. The area within hachures is stored in the computer.



not important until the incident wave has had a chance to reflect off the true interface and travel back to the artificial boundaries. Because of this, at the surface the contamination usually is present only in the later parts of the time series. The contamination due to both methods will reach any point at approximately the same time, but that produced by the free surface artificial-boundary condition should be larger and easier to recognize. Contamination is unavoidable, and the more easily it is recognized, the less chance there is of interpreting it as real motion. For this reason the free surface method for the artificial boundary is preferable to the use of solutions to an auxiliary problem.

The treatment of artificial boundaries is rather unsatisfactory and could stand much improvement. For single-frequency solutions, in contrast to the transient disturbances treated here, it may be possible to use some kind of impedance matching to terminate the space with reflectionless boundaries (Lysmer and Kuhlemeyer, 1969). Another possibility is to use numerical approximations to the absorbing mechanisms employed in laboratory wave tank experiments. As it now stands, in practice the artificial boundaries are placed as far from the region of heterogeneity as is economically feasible. Numerical experiments, using different distances to the sides and bottom, are essential to define the space–time region that is free of contamination.

## E. Initial Conditions

If a localized heterogeneity is surrounded by simple, plane-layered material, as in Fig. 6, an analytic solution for wave propagation in the plane layered media can be used to start the finite difference solution. If the initial

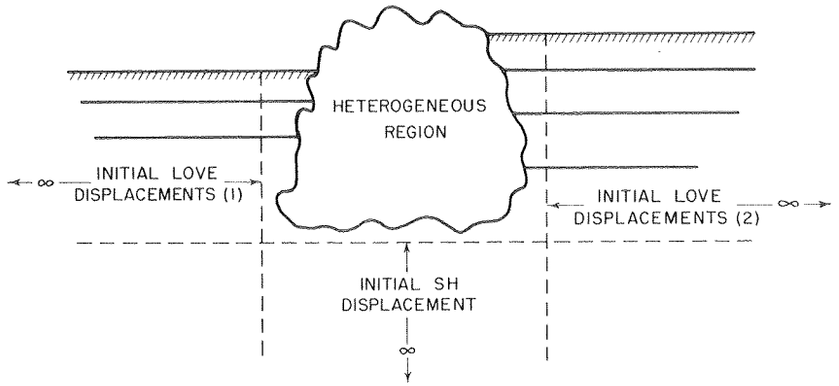


FIG. 6. A simple, source-free wave propagating into the region of heterogeneity. Waves commonly used as input are vertically incident SH body waves or Love surface waves of a given mode propagating on the waveguide to the right or left of the heterogeneity.

wavefield is zero in the region of heterogeneity, then by definition the equations of motion and boundary conditions throughout the medium will be satisfied. The transient disturbance is propagated through the region of interest by the numerical scheme. This hybrid approach insures that the input motion is free of unwanted phases. It is only in the specification of initial conditions that reference is made to a particular type of problem, such as Love surface waves or SH body waves; the equations of motion and boundary conditions are completely general. The difference scheme will give the total wave solution to the formulated problem as the initial disturbance propagates into the heterogeneous medium.

The basic characteristic of the input motions considered in this chapter is that they are set up by sources an infinite distance away, and thus are plane, source-free waves. This restriction is only for convenience. Converging or diverging waves, or waves from point or distributed sources within the medium, can also be included in the formalism without difficulty (e.g., Alterman and Karal, 1968; Alterman and Aboudi, 1970; Alterman *et al.*, 1972).

Although the principles hold for all types of input motion, most of the discussion below will focus on vertically incident, source-free plane SH waves with an impulse-like waveform. The use of the impulse waveform brings out some subtleties connected with the discrete nature of the grid through which the waves propagate.

### 1. *SH Body Waves*

a. *General Remarks.* In the following discussion, the discreteness effects mentioned above are ignored; if the input motions are distributed over a number of grid points, these are negligible, and experiments indicate that even for impulse-like initial functions the naive approach presented below can give adequate answers. An understanding of the influence of the discrete grid is important, however, in evaluating the results of the finite difference computations, and for this reason these effects are discussed at length in part c of this section.

Let the waveform of the input motion be given by $g(\xi)$. The solution $v_0$ for a vertically propagating, plane SH body wave in an infinite medium is then

$$v_0(z, t) = g(z + \beta[t - t_D]), \tag{20}$$

where $z$ is zero at the free surface and is positive downward, $\beta$ is the shear velocity in the lower medium, and $t_D$ is a time delay used to insure that the motion is essentially zero at the initial times in the region of changes in material properties. The basic approximation to the equation of motion, Eq. (8), requires displacements throughout the grid at time 0 and $\Delta t$ (or equivalently, displacement and velocity at $t = 0$) in order to propagate ahead in time. These initial displacements are given by the following scheme: first, $v^0_{m,n}$ and $v^1_{m,n}$ are set to zero for all $m, n$; second, for all grid points below the heterogeneous zone (which is usually a layer near the surface) the displacements are given by $v^0_{m,n} = v_0(n\,\Delta z, 0)$ and $v^1_{m,n} = v_0(n\,\Delta z, \Delta t)$ for all $m$'s. In effect, the continuous, infinite-media wavefield at two times is digitized in the horizontal and vertical directions.



b. *Impulse Approximation.* The form of $g(\xi)$ is quite arbitrary and until recently was chosen as a transient wavelet, discussed by Ricker (1945), with zero dc component and relatively narrow bandwidth in both wavenumber and spatial domains. In most cases, there were at least 20 grid points per dominant wavelength in the input motion. Because the results of the finite difference calculations are usually analyzed in the frequency domain, however, a more logical choice for an input function would be one possessing a broad frequency spectrum, and thus a short time (or space) extent. In addition to the broad frequency spectrum, there are several other desirable features associated with the short time duration. One is that the resulting seismograms are approximations to the impulse response of the model, and the various reflections and diffractions making up the motion are not smeared together as they are when a broad input motion is used; more information about the physics can then be obtained. Furthermore, the time delay term $t_D$ in Eq. (20) can be very small. This gives a reduction in the number of time steps needed to propagate the disturbance through the heterogeneous region as compared with the use of longer input motions with correspondingly larger time delays. Finally, the small spatial extent of the input motion allows the use of an expanding grid scheme such as discussed for Love waves in Section II,G,2.

If we attempt to use, as in Fig. 7, a true spike, the digitized displacement field at $t = \Delta t$ would be zero since the stability criterion discussed later requires that a wave move less than a grid spacing in a time $\Delta t$. The forward sense of direction of the wave is then lost, and backward propagating waves will result. Thus, we wish to use a spike-like function spread over several grid points; at the same time it would be desirable that the function possess continuous first and second derivatives. Both these objectives can be met by the following procedure (adapted from Alterman and Karal, 1968). Let

$$G_1 = \int_0^{\xi} \delta(\eta)\, d\eta = H(\xi), \tag{21a}$$

$$\vdots \qquad\qquad \vdots$$

$$G_4 = \int_0^{\xi} G_3(\eta)\, d\eta = \frac{\xi^3}{6} H(\xi), \tag{21d}$$

where $\delta(\eta)$ is the Dirac delta function and $H(\xi)$ is the Heaviside step function. $G_4$ has continuous first and second derivatives. We then take four consecutive centered finite differences over an arbitrary interval $L/4$ and normalize the result to unity at $\xi = 0$. This gives

$$\langle\delta(\xi)\rangle \equiv \frac{G_4(\xi + L) - 4G_4(\xi + L/2) + 6G_4(\xi) - 4G_4(\xi - L/2) + G_4(\xi - L)}{L^3/12} \tag{22}$$

as an approximation to the delta function which has continuous first and second derivatives and is zero for $|\xi|$ greater than $L$. Note that $\langle\delta(\xi)\rangle$ is a continuous function of $\xi$. To specify initial conditions on the discrete grid, we let $g(\xi) = \langle\delta(\xi)\rangle$. A convenient measure of the width of $g$ is then $L/\Delta z$.

c. *Effects of a Discrete Grid.* There are two effects associated with the use of a discrete grid which should be remembered when analyzing results of the computations: the aliasing of the continuous time series, and the dispersion of waves propagating on a lattice.

The aliasing effect can be explained best by referring to Fig. 7, where the digitized form of a spike at times 0 and $\Delta t$ is given by the solid circles.

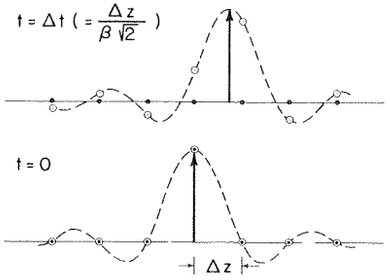


FIG. 7. A spike and the corresponding function which has no power above the Nyquist wavenumber $\pi/\Delta x$, at two consecutive times. The closed and open circles are the digitized forms of the spike and its corresponding function.

The problem is that the amplitude spectra of the two discrete time series will be different; it will be flat for $t = 0$ and zero for $t = \Delta t$. As shown in the figure, however, the discrete values at $t = 0$ could also come from the function

$$\text{sinc}\ \xi \equiv [\sin(\pi/\Delta z)\xi]/(\pi/\Delta z)\xi. \tag{23}$$

This has a flat spectrum up to the Nyquist wavenumber ($k_z = \pi/\Delta z$) and is zero thereafter, and it is not aliased by the digitization. The result of using this function to generate the displacements at $t = \Delta t$ is given by the open circles in the upper part of Fig. 7. The two open-circle time series have the same amplitude spectra and are therefore consistent representations of the input motion.



Generalizing the discussion above to an arbitrary form of the input motion, it follows that sinc* $\langle\delta(\xi)\rangle$ (where * represents convolution) should be used, in place of Eq. (22), to generate the input motion. The result of neglecting the aliasing effect is to produce as initial input a mixture of propagating waves rather than the single source-free wave desired; this mixture will produce undesirable modulation in the wavenumber or frequency domains. Obviously, the effect of aliasing will diminish as less power above the Nyquist wavenumber is included in the spectrum of the continuous input function $g(\xi)$. The Ricker pulses used in computations were chosen such that they had virtually no power above Nyquist, and thus the effect above was negligible.

Another problem encountered by short duration pulses is that the velocity used to advance the input motion at $t = 0$ to $t = \Delta t$ is dependent on wavenumber for waves propagating on a discrete lattice (Brillouin, 1953). This dispersion is shown in Fig. 8 for waves on a one-dimensional spring-mass

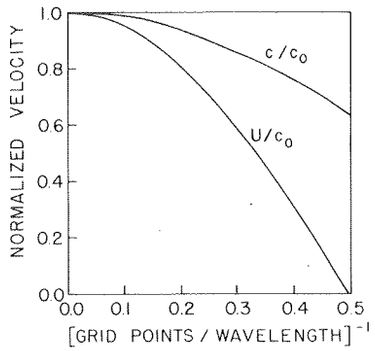


FIG. 8. Phase ($c$) and group ($U$) velocities for wave propagation on a simple spring-mass system. $c_0$ is the phase velocity for propagation in the corresponding continuous media. The abscissa is equivalent to the product of wavenumber and grid spacing.

system. The dispersion becomes important for 10 or fewer grid points per wavelength. This illustration also emphasizes that even if the initial conditions are calculated so as to take the aliasing and the dispersion into account, care must be taken, in analyzing the results, to separate the effects due to the discrete nature of the actual problem being solved from the real effects of the physical problem we are attempting to model. In practice, this would probably mean neglecting all information for frequencies higher than some arbitrary cutoff value.

A possible way of including the aliasing and dispersion effects in the initial displacements is to first specify $v^0_{m,n}$ in the usual way from $\langle\delta(\xi)\rangle$ and then take a Fast Fourier Transform (FFT) over the $z$-index $n$. (Because of the vertical incidence and plane wave, $v^0_{m,n}$ is independent of $m$; thus, only

one transform is required.) The corresponding spectrum is then advanced by the phase factor $\exp[jk_l c(k_l)\,\Delta t]$, where $k_l$ are discrete wavenumbers and $c(k)$ is the discrete grid phase velocity, and then resynthesized with another FFT to produce $v^1_{m,n}$ for all $n$'s.

### 2. *Love Surface Waves*

Although the above discussion also applies to Love waves, or for that matter to any other input motion, the effects of the discrete grid will now be ignored in order to concentrate on another aspect of the input motion. Because Love waves are inherently dispersive, the main problem in specifying the initial conditions is evaluating the function $v_0(x, z, t)$. This can be done easily by using the eigenfunction of the problem in combination with a FFT to synthesize a traveling wave solution such that $v_0(x, 0, 0) = g(x)$, where $g(x)$ is an arbitrary waveform. It is most convenient to take the FFT over discrete wavenumbers which are consistent with the grid spacing $x$, for then at a specified depth and time one FFT will give the displacements at all horizontal grid points. If $NZ$ is the number of grid points in the vertical direction, $2 \cdot NZ$ Fast Fourier Transforms will be required for the generation of the initial conditions.

## F. Truncation, Stability, and Convergence

We would like to guarantee that solutions to the difference equations remain bounded as the computations proceed (that is, errors at a given time step do not become magnified) and further, that as we make the grid spacings smaller and smaller these solutions approach the solution of the differential equation. Rigorous treatment of such matters is beyond the scope of this chapter, but some useful and informative results can be derived from simpler analysis.

### 1. *Truncation*

A measure of truncation error in a finite difference approximation is given by inserting the solution to the corresponding differential equation into the difference approximation. If the error approaches zero as the grid spacing decreases, then the difference approximation is said to be consistent with the differential equation. To study this, let $\tilde{v}(x, z, t)$ be a solution to Eq. (6). Since most of our problems involve composite materials made of homogeneous media, we assume for convenience that $\mu$ is a constant. By expanding $\tilde{v}$ in a Taylor series, evaluating it at the grid points used in the finite difference approximation of the differential equation, and using the



second time derivative of the wave equation to find an expression for $\partial^4\tilde{v}/\partial t^4$, the truncation error in the difference equation can be written

$$\begin{aligned}\text{error} &\equiv \{\delta_t{}^2\tilde{v} - \beta^2[\delta_x{}^2\tilde{v} + \delta_z{}^2\tilde{v}]\}_{m,n} \\ &= \frac{\beta^2}{12}\left\{[\beta^2\,\Delta t^2 - \Delta x^2]\left[\frac{\partial^4\tilde{v}}{\partial x^4} + \frac{\partial^4\tilde{v}}{\partial z^4}\right] + 2\beta^2\,\frac{\partial^4\tilde{v}}{\partial x^2\,\partial z^2}\,\Delta t^2\right\}_{m,n} \\ &\qquad + O(\Delta t^4, \Delta x^4) \qquad (24)\end{aligned}$$

where $\Delta x = \Delta z$ and $\delta_t{}^2$, $\delta_x{}^2$, and $\delta_z{}^2$ are difference operators defined by Eq. (2). The truncation error approaches zero as $\Delta x, \Delta t \to 0$, and thus the equations are consistent.

If $\partial^4\tilde{v}/\partial x^2\,\partial z^2 = 0$, as it is when the motion is in one direction only, the choice $\beta\,\Delta t = \Delta x$ will cause the second-order error term in Eq. (24) to vanish. For one-dimensional motion the stability condition, as shown below, is $\beta\,\Delta t \leqq \Delta x$. Thus, for a given $\beta$ and $\Delta x$, $\Delta t$ should be taken close to its upper limit. For general two-dimensional motion the mixed derivative is not zero, and the error term cannot be made to vanish by a judicious choice of the grid spacing. In fact, the relation $\beta\,\Delta t = \Delta x$ violates the stability condition for two-dimensional motion. Letting $\Delta t$ be close to its upper limit, however, is probably the optimum choice, as it will make the first term of the error as small as possible.

### 2. *Stability*

The easiest way of investigating stability is to use the Fourier series approach pioneered by von Neumann (O'Brien *et al.*, 1950). This, however, does not consider the effect of boundary conditions, and therefore a different technique based on matrices will be used (see, e.g., Smith, 1965). Let $\mathbf{v}^p$ be a vector with the node point displacements at time $p$ as elements. The equations of motion and interface conditions can be combined in the matrix equation

$$\mathbf{v}^{p+1} = \mathbf{A}\mathbf{v}^p + \mathbf{B}\mathbf{v}^{p-1}, \qquad (25)$$

where $\mathbf{A}, \mathbf{B}$ are matrices to be given later, and the superscript, as usual, stands for the time level at which the displacements are evaluated. By defining, in block notation,

$$\mathbf{u}^p = \begin{pmatrix}\mathbf{v}^p \\ \mathbf{v}^{p-1}\end{pmatrix} \qquad (26)$$

and

$$\mathbf{P} = \begin{bmatrix}\mathbf{A} & \mathbf{B} \\ \mathbf{I} & \mathbf{0}\end{bmatrix}, \qquad (27)$$

where **I** and **0** are identity and null matrices, we can rewrite Eq. (25) as

$$\mathbf{u}^{p+1} = \mathbf{P}\mathbf{u}^{p}. \tag{28}$$

A necessary condition that the errors at some time step do not become magnified with time is that the eigenvalues, $\lambda$, of **P** be less than or equal to 1.0 in magnitude. If $\eta$ is an eigenvalue of **A**, Fox (1962) shows that $|\eta| \leqq 2$ implies $|\lambda| \leqq 1$. If we write out the elements of **A** for the difference approximation of Eq. (6), assume $\Delta x = \Delta z$, and use Gershgorin's theorem (Mitchell, 1969), the following stability condition is found:

$$\langle\beta\rangle\, \Delta t/\Delta x \leqq 1/\sqrt{2}, \tag{29}$$

where

$$\langle\beta\rangle^2 = \tfrac{1}{4}(\mu_{\mathrm{N}} + \mu_{\mathrm{S}} + \mu_{\mathrm{E}} + \mu_{\mathrm{W}})/\rho. \tag{30}$$

The $\mu_{\mathrm{N,S,E,W}}$ are the equivalent rigidities at the node points in the computational star surrounding any arbitrary point at $m\,\Delta x$, $n\,\Delta z$. Equation (29) is important and accurately predicts when instabilities will occur. For a uniform material it is identical to the stability condition found from von Neumann's method.

In a completely nonuniform material, $\langle\beta\rangle$ would be a nonconstant function of $(x, z)$. All of our applications, however, involve uniform materials and thus $\langle\beta\rangle$ will be constant over most of the grid; it will change locally only in the vicinity of the interfaces between the media. This means that in practice we can use Eq. (29) with $\langle\beta\rangle$ replaced by the highest uniform media velocity, $\beta_{\max}$, present in the model. Furthermore, inspection of the formulas for $\mu_{\mathrm{N,S,E,W}}$ show that $\langle\beta\rangle \leqq \beta_{\max}$ and thus no instability should arise from the interface when it is treated as a heterogeneous material. When the explicit continuous stress method is used, on the other hand, the asymmetric difference approximations to the Laplacian near the interface use short internodal distances. If $\Delta t$ has been determined on the basis of both the maximum velocity and the minimum $\Delta x$ or $\Delta z$ of the regular rectangular network, then the short internodal distances will cause local violations of the stability conditions, and an instability can arise. The instability will grow away from the point of initiation, and will eventually swamp the whole grid. This is different from the result found when Eq. (29) does not hold over a wide area, for then, although the instability may start in several local regions, it almost immediately spreads to the entire area. In either case, the use of a time marching scheme enables one to see when and where an instability arises,



and it often happens that usable solutions can be obtained in a problem which is eventually overwhelmed by an instability.

As a final remark, the stability condition for a uniform medium of $n$ space dimensions is

$$\beta\, \Delta t/\Delta x \leqq 1/\sqrt{n}. \tag{31}$$

Thus, for a given grid spacing, going to higher dimensions requires smaller time steps and proportionately more computation time. This is of minor importance, however, when compared to the increase of time resulting from the increase in the number of grid points.

### 3. *Convergence*

Convergence exists if the solution to a difference equation approaches the solution of the corresponding differential equation as the mesh is refined. For consistent difference equations, convergence is often intimately associated with stability; for one-dimensional wave propagation in an unbounded medium the conditions for convergence are precisely those for stability (Fox, 1962). Two-dimensional, bounded domain problems are more difficult to treat, but numerical experiments again show that for all practical purposes the existence of stability implies convergence.

## G. Computational Details

One of the appealing features of the finite difference method presented on the previous pages is the ease with which it can be programmed. Because of this, only a few details of the programming will be discussed.

### 1. *Storage Space*

Because we need displacements at two time levels, $p$ and $p-1$, in order to calculate the values at the next time step, it would seem at first glance that we require storage spaces for three time levels [i.e., $(3)(NX)(NZ)$ spaces, where $NX$, $NZ$ are the number of grid points in the $x$, $z$ directions]. Since, however, $v^{p-1}_{m,n}$ is only used once, in the calculation of $v^{p+1}$ at $m$, $n$, the storage locations occupied by the displacements at the $p-1$ time level can be used for the new values. Then only $(2)(NX)(NX)$ spaces are required in the array of displacement values.

Another comment about storage concerns the weighting factors ($\mu_{\mathrm{N,S,E,W}}$) in the finite difference approximation of the heterogeneous wave equation. These factors are most logically computed before the time marching proceeds. If the medium is completely heterogeneous it is necessary to store four

weighting factors at each grid point. This is an important limitation on the usefulness of the technique if a large amount of storage space is not available. In regions of homogeneous material, however, the weighting factors are constant and it would be redundant to store them all. Then it is most practical to define the heterogeneous regions by an array of indices, and store the weight factors in corresponding arrays. When sweeping the grid in the time marching process, the new displacements are computed first for all the homogeneous regions using Eq. (8). After this, Eq. (11) or Eq. (16) is used with the previously determined weighting factors to calculate the rest of the new values.

2. *Expanding Grid*

Because many grid values are initially zero, only a steadily increasing portion of the entire grid need be swept at each time iteration. This is especially important in the case of Love waves, where typically the initial displacements are contained horizontally within 100 points but 200 more points represent the medium into which the wave is to propagate. Sweeping all 300 horizontal grid points at each iteration would needlessly waste much computation time. The expanding grid concept as applied to Love wave propagation is shown schematically in Fig. 9. As shown, the reasoning also can be extended to "bring up the rear" of the Love waves. Since reflected waves are expected, however, this is not as justified as pushing out the front. In practice, the rear is brought up at a slower rate than the front is advanced, and is stopped at a predetermined point ($m_{\text{stop}}$ in the figure) to allow for reflected waves in the vicinity of the inhomogeneity. This scheme of pushing out the front and bringing up the rear results in a considerable saving of time. Storage space can be saved also by continually backfilling the displacements into the leftmost unused portions of the grid.

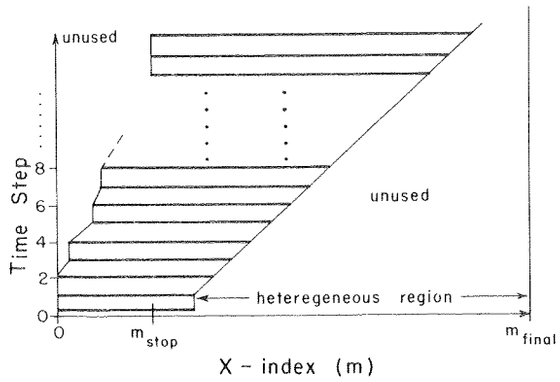


FIG. 9. The expanding grid scheme for Love wave propagation. At any given time step displacements are computed for the horizontal portion of the grid indicated by solid lines. All vertical grid points are used at each time step.



3. *Output*

Two kinds of output are commonly used. Printer–plot "snapshots" of the motion, generated at given times, are the first type and are useful as a qualitative check on the progress of the solution. In particular, these snapshots are very useful in looking for instabilities. Displacement values from "seismometers" located at arbitrary positions in the medium are the second type of output. These are stored at predetermined time intervals and, after completion of the time cycles, are punched on cards to be used in subsequent analysis. Most of the subsequent analysis is done in the frequency domain and usually involves computations of phase velocities in the Love wave experiments and spectral ratio determinations for the SH body-wave results. Examples are given later.

## III. Extensions of the Method

Many more techniques and possible applications exist than indicated by the development above. Discussed below are some which should prove useful in seismology.

### A. Viscoelastic Problems

Chiu (1965) and Alterman and Aboudi (1969) have done some computations using simple Maxwell and Voigt viscoelastic models, apparently with no difficulty. Explicit schemes can be used for both, but the difference approximation for the Voigt model, as compared with the perfectly elastic case and Maxwell model, uses $v_{m,n}^{p-1}$ more than once in computing displacements at the time level $p+1$. By the proper use of temporary storage locations, however, still only two levels of storage for the displacement field are required.

The stability criteria for the simplest approximation to the Voigt equations is given by

$$\beta\, \Delta t/\Delta x \leqq (1/\sqrt{2})[1/1 + (DN/\pi)]^{1/2}, \tag{32}$$

where $D$ is the fractional damping ratio and $N$ is the number of points per wavelength. The formula above is adapted from one given by Alterman and Aboudi (1969) and is valid for all practical values of $D$ and $N$. This stability condition is not overly restrictive. For the explicit Maxwell scheme, the stability condition is essentially that given by Eq. (29).

### B. Crack Problems

Several successful applications of the finite difference technique to crack problems have been reported by Alterman *et al.* (1972) and, using a more complicated scheme than developed in this chapter, by Hanson and Sanford (1970) and Hanson *et al.* (1971). The simulation of crack propagation in complex materials could be easier and less costly than source-free problems since the artificial boundaries are of lesser importance and the generation of initial conditions need not use complicated computations, such as Fourier transforms, at a large number of grid points.

### C. Hybrid Schemes

As has been emphasized, the finite difference technique is most useful in near-source calculations, whether these be real sources such as above, or secondary sources caused by heterogeneities. For secondary sources, our primary concern, a hybrid approach was used in which analytic solutions for uniform or simply layered material were propagated by the finite difference method through locally inhomogeneous regions. A more complete hybrid approach would then use the resulting wave fields and propagate these through the remaining uniform media in an analytic manner. In this way we could evaluate the effect of a given heterogeneity at any arbitrary distance. The question is: how do we continue the finite results? A representation theorem could be used from which $v$ at an arbitrary point in space could be found given $v(t)$ on some surface enclosing the heterogeneities. The surface values would be given by the finite difference results. The implementation of this may be difficult, and it might be more practical to decompose the total computed motion into various components with known modes of propagation. As an example, in the case of two plane-layered waveguides joined by a heterogeneous region (as in Fig. 6), an attempt could be made to break down the motion on the far side into leaking and trapped modes. The trapped modes could then easily be propagated analytically. A problem in such decompositions is finding an orthogonality condition that will separate the trapped from leaky energy. Alsop (1968) discusses this.

## IV. Numerical Experiments and Examples

The examples to be presented are intended to illustrate various features of the finite difference method, not the physics of the problems considered. The physical significance of the results are given in Boore (1970b, 1972) and Boore *et al.* (1971). All computations were performed in single precision arithmetic on either an IBM 360/65 or IBM 360/67 computer.



### A. Love Waves

#### 1. *Plane-Layered Models*

It is important to test the numerical method on problems for which independent answers are available. Toward this end, several problems of Love wave propagation on one- and two-layered half-spaces were solved. The Love wave calculations used a grid with internode spacing which, after a given depth, increased with distance in the downward direction. The purpose was to take advantage of the decay with depth of the Love wave displacements in order to increase the time interval at the surface before spurious reflections from the bottom contaminated the solution. This device seemed to work for the problems considered, but Lysmer (1971) and Frizonnet (1970) reported that in other problems spurious reflections were produced at the point where the increased scaling with depth started.

Time series computed by the finite difference method and by the synthesis of the theoretical eigenfunctions were saved at several sites spaced at equal intervals along the surface. Fourier transforms of these time series were used to compute intersite phase velocities and amplitude ratios (normalized to the first site encountered by the wave). The results for a model with a low velocity zone, given in Fig. 10, show excellent agreement between theory and computation. At the high and low ends of the spectrum the small amount of power in the input motion produces scatter in the results, but this is encouragingly small.

Of interest is whether the inaccuracies in the computations are steadily increasing with time or tend to damp out. The extreme case of instability is easy to recognize, of course, but a gradual loss of accuracy is not. To study this, the wavenumber spectra of the surface displacements for a model with a single layer over the half-space were compared, at different times, with theory. The error was investigated in the wavenumber rather than the frequency domain since the displacements throughout the grid at any fixed time represent the same number of algebraic manipulations. This is opposed to the time series at a given node point, in which each value represents a different number of computations. Because, however, the error propagates as a wave, the ideal would be to study the error spectrum in frequency–wavenumber space.

The percent error in the computed wavenumber spectral amplitudes are given as a function of time and wavenumber in the last three columns of Table I. The first column contains the wavenumber and the second column contains, for reference, the theoretical amplitude for each wavenumber. This table shows that the error in amplitude is small, that the relative error (e.g., error at $t = 84$ sec compared to that at $t = 42$ sec) increases with time,

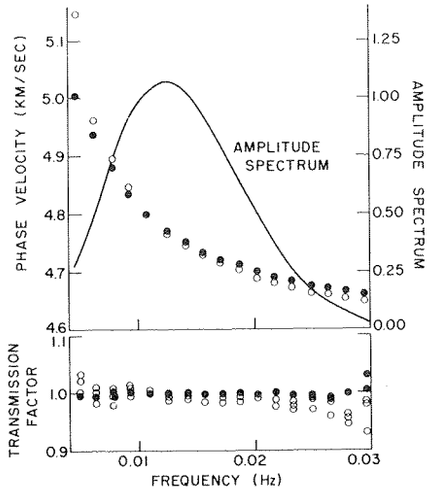


FIG. 10. Love surface wave propagation on a model with a low velocity layer. Phase velocities were computed between three stations spaced 120 km apart. The model was $\beta_1, \beta_2, \beta_3, = 4.75, 4.55, 5.20$ km/sec; $\rho_1, \rho_2, \rho_3 = 3.3, 3.4, 4.0$ g/cc; layer thicknesses 100 and 200 km. Computational parameters were $\Delta x = 10.0$ km, $\Delta t = 1.25$ sec, and $NZ = 60$ (includes scaling of grid spacing with depth). ● Theoretical, ○ calculated.

TABLE I

PERCENT ERROR IN AMPLITUDE AS A FUNCTION OF WAVENUMBER AND TIME[a,b]

| $k$ | Theoretical amplitude | $t = 42$ sec | $t = 84$ sec | $t = 126$ sec |
|---|---|---|---|---|
| 0.012 | 0.15 | −0.4 | −1.2 | −1.9 |
| 0.024 | 0.35 | −1.6 | −2.2 | −2.9 |
| 0.037 | 0.30 | −2.4 | −3.4 | −4.5 |
| 0.049 | 0.15 | −2.5 | −4.1 | −4.5 |

[a] Physical model: $\beta_1$, $\beta_2 = 3.85$, 4.75 km/sec; $\rho_1$, $\rho_2 = 3.00$, 3.65 g/cc; $H = 15$ km. Computational parameters: $\Delta x = 5$ km; $\Delta t = 0.7$ sec.

[b] Adapted from Boore (1970b).



and that the computed amplitudes are consistently lower than the theoretical amplitudes. The phase spectra errors, not given here, show a consistent, small bias which imply an overestimation of phase velocity, but they do not increase in an obvious way with time.

As a final example of a problem having an analytical solution, the computer generated results for a model of two layer–half-space combinations joined by a vertical boundary are shown in Fig. 11. (This problem has an analytical solution only if certain relations between the physical parameters are satisfied.) Printer plot "snapshots" are given at several instances of time and clearly show the reflected and transmitted waves caused by the interaction of the incident motion with the vertical interface. The computed results and the theoretical results agree to within a few percent.

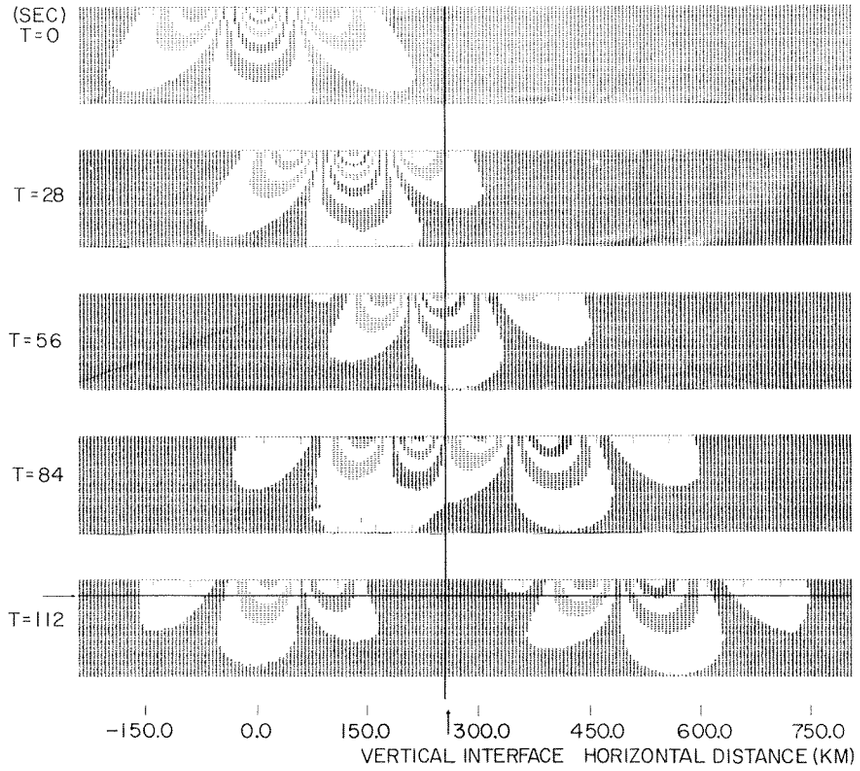


FIG. 11. Printer-plot contours of Love wave propagation in a model with two layer–half-space combinations joined along a vertical interface. The interfaces are shown by solid lines (the horizontal interface is shown only once).

### 2. *Sloping Layer Models*

The model shown at the bottom of Fig. 12 is a representation of an ocean–continent boundary. Two types of input were used, one with the waves propagating to the right (updip) and one to the left (downdip). Phase velocities were computed between the stations shown over the region of thickness change, with the results shown in the upper part of the figure. The interface

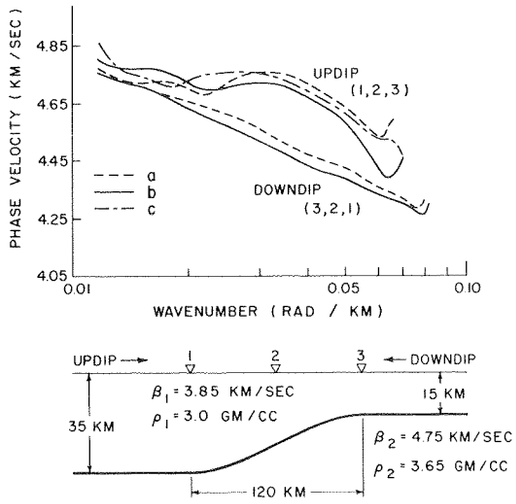


FIG. 12. Phase velocities measured over the region of thickness change for Love wave propagation. See text for the explanation of curves a, b, and c.

was treated by the explicit continuous stress method (curve a), a generalization of this using higher order approximations to derivatives (curve b), and the regular explicit continuous stress method with a smaller grid spacing ($\Delta x = 3.0$ km rather than 5.0 km; curve c). In this problem no analytical answers are available; the close similarity of the results, however, gives reassurance that the distinct nonreciprocity in measured phase velocities is real and not a peculiarity of the numerical method.

## B. SH Waves—Vertical Incidence

### 1. *Basin Problems*

In the examples below the basins are symmetrical about the left boundary, and thus only half the solution field is shown. Printer-plot contours of displacement are shown in vertical sections at four instants of time in Fig. 13.



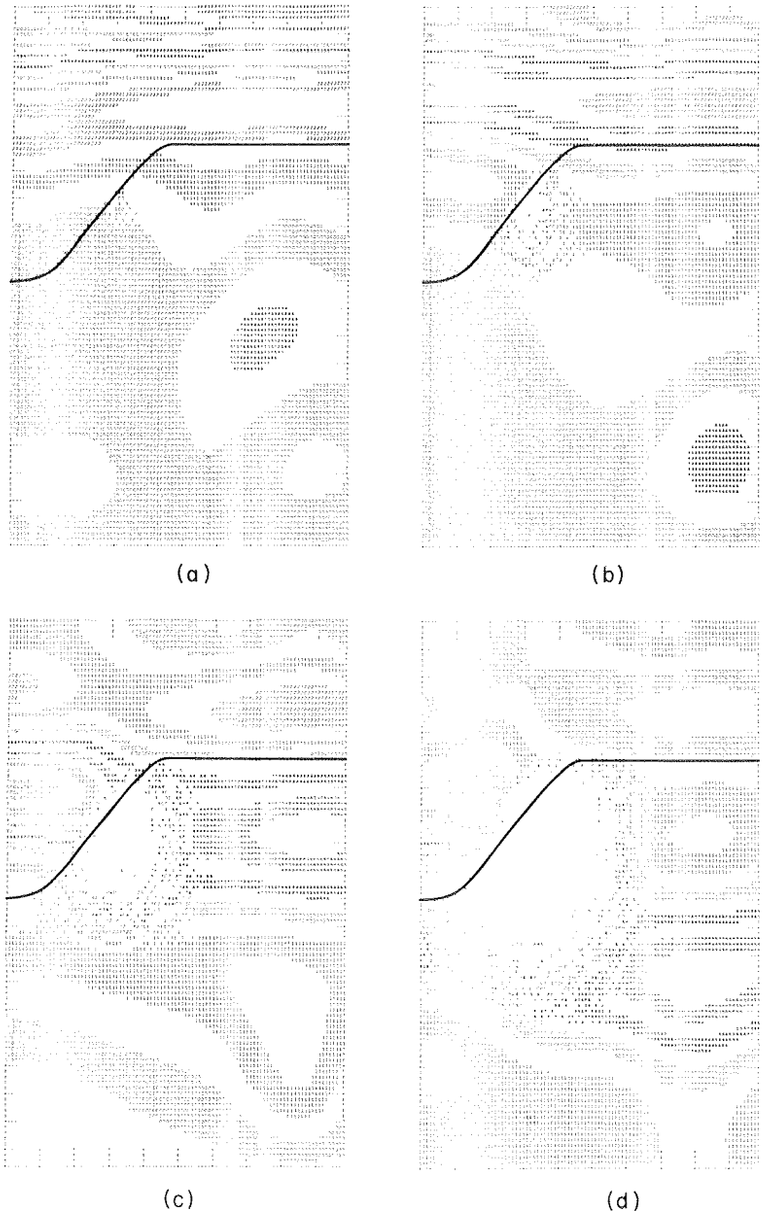


FIG. 13. Contour plots at times (a) 5.0, (b) 6.0, (c) 7.0, and (d) 8.0 sec for a SH wave vertically incident on a basin [see Figure 2 in Boore *et al.* (1971) for plots at earlier times]. The growth of a local instability is shown by the expanding blank area. Physical parameters: $\Delta x = 0.2$ km, $\Delta t = 0.025$ sec.

The explicit continuous stress method was used to treat the interface in this problem, and because of the short legs in the computational star near the interface a local instability was produced. The spreading blank area in the figure (blank because the numbers were outside the specified range of contour values) represents the growth of this instability.

The model in Fig. 13 had a relatively steep walled basin and had velocities appropriate to the crust–upper mantle interface. Of more interest to earthquake engineering is the symmetric basin, filled with low rigidity sediments, shown in Fig. 14. The computed motion at the surface over the center of the basin and the auxiliary solution are shown in the upper part of Fig. 14. The dashed time series is the solution to the one-dimensional problem obtained by replacing the basin by a layer of uniform thickness equal to the maximum basin thickness; this is known as the flat layer approximation (FLA). The Fourier spectrum of each trace was computed, and spectral ratios were formed

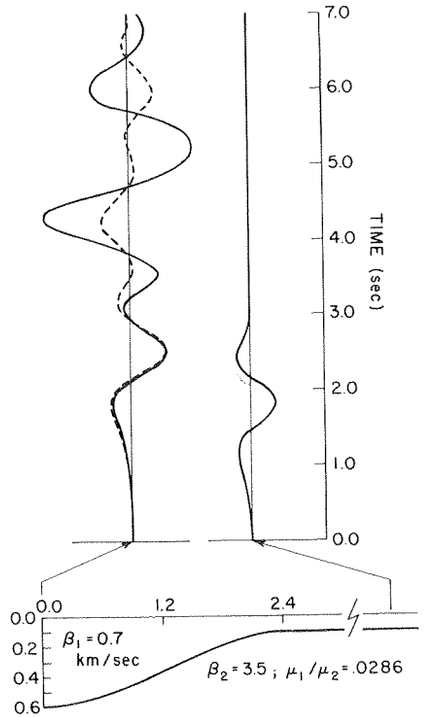


FIG. 14. Computed seismograms at the surface of a basin filled with low velocity sediments. The seismogram on the right is the reference trace, computed from the auxiliary problem, to which the other time series are compared. The dashed curve is from the flat layer approximation.



by dividing by the spectrum of the auxiliary solution. The amplitude spectra of the two solid-line time series in Fig. 14 are shown in the top of Fig. 15, and the amplitude ratios are given in the lower part of the figure. The circles are results from a completely different method for solving the problem (Aki and Larner, 1970). The excellent comparison gives confidence in the finite difference results.

The basin problem was solved using the explicit continuous stress method and also the three heterogeneous material approaches implied in Fig. 2; the results were all in good agreement. Because abnormally small time steps were not required by the presence of local instabilities, the heterogeneous material runs were four times faster than the explicit continuous stress computations. The heterogeneous approach took a little over 3 min of

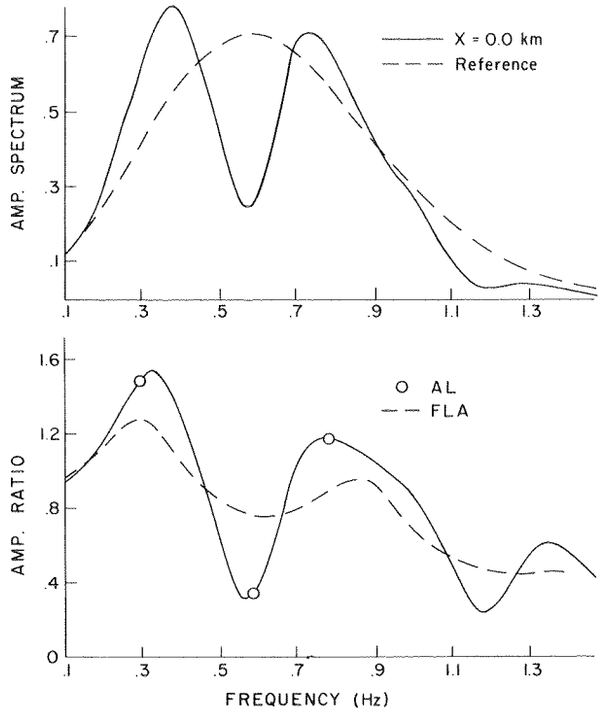


FIG. 15. Frequency-domain comparison of the results in Fig. 14. The amplitude spectra at the top as divided to produce the solid-line curve at the bottom. The open circles are from the independent method discussed by Aki and Larner (1970). For comparison purposes, the time series were multiplied by an exponential window before Fourier analysis; this is equivalent to propagation in a material having damping which increases with period. Adapted from Boore *et al.* (1971).

IBM 360/67 execution time for 350 time steps on a 75 × 100 grid. Accurate solutions could undoubtedly be obtained with larger grid spacings, thereby reducing the computation time.

## 2. *Topography Problem*

A semi-infinite medium with surface topography is shown in Fig. 16. The ramp, step nature of the surface resulted from the method used for the free surface boundary condition; another run with a coarser representation of the surface gave the same answers, implying that to the incident waves

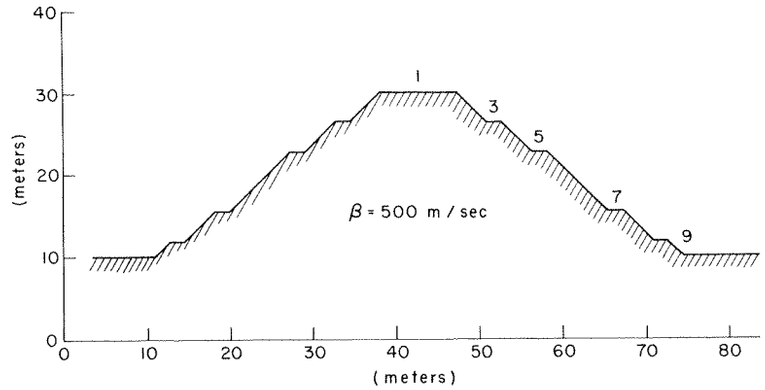


FIG. 16. A model of topograph relief. The ramp-step nature of the surface is a result of the method used to treat the free surface boundary condition. Computational parameters: $\Delta x = 2.0$ m, $\Delta t = 0.0014$ sec.

the surface is smooth. The resulting seismograms at several points along the surface are shown in Fig. 17 for an initial Ricker wavelet and for a spike approximation. It is obvious that the spike computations require only about half as many time steps as the Ricker results. The spike results also show much more clearly the second arrival due to reflection of the incident pulse on the far side of the surface bump. The amplitude spectra and spectral ratios for three input motions—two Ricker wavelets of differing spectral content and the spike approximation—are given in Fig. 18. This figure again shows the usefulness of the spike, for one run gives information over a broader spectral band than the two Ricker runs. The small modulation in the spike results is probably due to discreteness effects, as discussed in Section II,E,1. The initial input motion was not corrected for these effects. Apparently the difficulties in generating the initial displacements for a spike-like input are not as important as they might seem at first.

The problem defined in Fig. 16 was also solved, unintentionally, with a



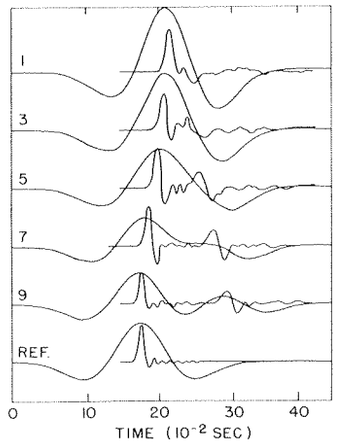


FIG. 17. Computed seismograms at points shown in Fig. 16 for two types of input motion: Ricker wavelet and impulse approximation. Some of the high frequency oscillations are due to dispersion.

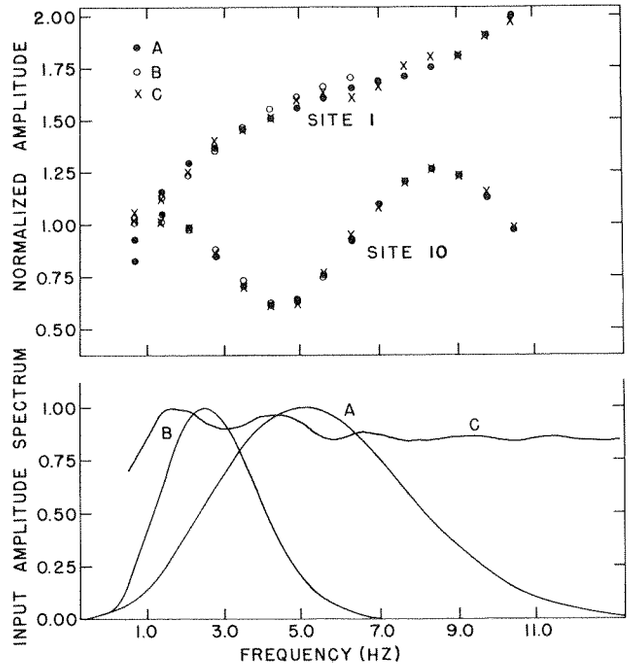


FIG. 18. Results for the model of topographical relief. Lower: The amplitude spectrum of the input motion—two Ricker wavelets (A, B) and an impulse approximation (C). Upper: The resulting spectral ratios, normalized to the surface motion obtained if no topography were present, at sites 1 and 10 (see Fig. 16; site 10 is just to the right of site 9).

spike representation possessing a discontinuous second derivative [i.e., the third difference of $G_3$; see Eq. (21)]. Even though the breadth of the input pulse was the same as in the previous spike run ($L/\Delta z = 4$), the results were distinctly poorer.

### Acknowledgments

I wish to thank Bill Joyner for a number of helpful discussions and also for suggesting some valuable improvements on the manuscript. Judy Boore was of immeasurable help in providing technical assistance. I also wish to thank the American Geophysical Union for permission to reproduce and adapt several figures and a table from my previous publications.

This chapter was prepared while I was an NRC-USGS Post-Doctoral Research Associate and was done in cooperation with the Division of Reactor Development and Technology ,U.S. Atomic Energy Commission. Publication authorized by the Director, U.S. Geological Survey.

### References

Aki, K., and Larner, K. L. (1970). *J. Geophys. Res.* **75**, 933.
Alsop, L. E. (1968). *Bull. Seismol. Soc. Amer.* **58**, 1949.
Alterman, Z. S., and Aboudi, J. (1969). *Isr. J. Technol.* **7**, 135.
Alterman, Z. S., and Aboudi, J. (1970). *Geophys. J. Roy. Astron. Soc.* **21**, 47.
Alterman, Z. S. and Karal, F. C., Jr. (1968). *Bull. Seismol. Soc. Amer.* **58**, 367.
Alterman, Z. S., Burridge., R. and Loewenthal, D. (1972). *Geophys. J. Roy. Astron. Soc.* (in press).
Bertholf, L. D. (1967). *J. Appl. Mech.* **34**, 725.
Bhattacharyya, B. K. (1969). *Geophysics* **34**, 402.
Boore, D. M. (1970a). Ph.D. Thesis, Massachusetts Institute of Technology, Cambridge.
Boore, D. M. (1970b). *J. Geophys. Res.* **75**, 1512.
Boore, D. M. (1972). *Bull. Seismol. Soc. Amer.* (in press).
Boore, D. M., Larner, K. L., and Aki, K. (1971). *J. Geophys. Res.* **76**, 558.
Brillouin, L. (1953). "Wave Propagation in Periodic Structures." Dover, New York.
Cherry, J. T., and Hurdlow, W. R. (1966). *Geophysics* **31**, 33.
Chiu, S. S. C. (1965). Ph.D. Thesis, Penn. State University, University Park.
Claerbout, J. F. (1970a). *Geophysics* **35**, 407.
Claerbout, J. F. (1970b). *In* "Acoustical Holography" (A. F. Metherell, ed.), Vol. 3, p. 273. Plenum Press, New York.
Claerbout, J. F. (1971) *Geophysics* **36**, 467.
Claerbout, J. F., and Johnson, A. G. (1972). *Geophys. J. Roy. Astron. Soc.* (in press).
Curtis, A. R., and Shimshoni, M. (1970). *Bull. Seismol. Soc. Amer.* **60**, 1077.
Fox, L. (1962). "Numerical Solution of Ordinary and Partial Differential Equations." Pergamon, Oxford.
Frizonnet, J. M. (1970), Written communication.
Hanson, M. E., and Sanford, A. R. (1970). *Bull. Seismol. Soc. Amer.* **60**, 1209.
Hanson, M. E., Sanford, A. R., and Shaffer, R. J. (1971). *J. Geophys. Res.* **76**, 3375.
Landers, T. (1971). Ph.D. Thesis, Stanford University, Stanford, California.
Larner, K. L. (1970). Ph.D. Thesis, Massachusetts Institute of Technology, Cambridge.
Lysmer, J. (1971). Oral communication.
Lysmer, J., and Kuhlemeyer, R. L. (1969). *J. Eng. Mech. Div. ASCE* **95**, 859.



Maenchen, G., and Sack, S. (1963). Lawrence Radiat. Lab. Rep. UCRL-7316.
Mitchell, A. R. (1969). "Computational Methods in Partial Differential Equations." Wiley, New York.
Moler, C. B., and Solomon, L. P. (1970). *J. Acoust. Soc. Amer.* **48**, 739.
O'brien, G. G., Hyman, M. A., and Kaplan, S. (1950). *J. Math. Phys. (Cambridge, Mass.)* **29**, 223.
Petschek, A. G., and Hanson, M. E. (1968). *J. Comp. Phys.* **3**, 307.
Plamondon, M. A. (1966). Ph.D. Thesis, University of Illinois, Urbana.
Richtmeyer, R. D., and Morton, R. W. (1967). "Difference Methods for Initial-Value Problems." Wiley (Interscience), New York.
Ricker, N. (1945). *Geophysics* **10**, 207.
Rowe, P. P. (1955). *Trans. Amer. Geophys. Un.* **36**, 995.
Schoenberg, J. J. ed. (1969), "Approximations With Special Emphasis on Spline Functions." Academic Press, New York.
Shimshoni, M., and Ben-Menahem, A. (1970). *Geophys. J. Roy. Astron. Soc.* **21**, 285.
Smith, G. D. (1965). "Numerical Solution of Partial Differential Equations." Oxford Univ. Press, London and New York.
Wesson, R. L. (1971). *Trans. Amer. Geophys. Un.* **52**, 284.